THE DYNAMICS OF REGULARISED DISCONTINUOUS MAPS WITH APPLICATIONS TO IMPACTING SYSTEMS

S.R. PRING*AND C.J. BUDD*†

Abstract. One-dimensional piecewise-smooth discontinuous maps (maps with gaps) are known to have surprisingly rich dynamics, including periodic orbits with very high period and bifurcation diagrams showing period-adding or period-incrementing behavour. In this paper we study a new class of maps, which we refer to as regularised one-dimensional discontinuous maps, because they give very similar dynamics to discontinuous maps and closely approximate them, but are yet continuous. We show that regularised discontinuous maps arise naturally as limits of higher dimensional continuous maps when we study the global dynamics of two non-smooth mechanical applications: the cam-follower system and the impact oscillator. We review the dynamics of discontinuous maps, study the dynamics of regularised discontinuous maps and compare this to the behaviour of the two mechanical applications which we model. We show that we observe period-adding and period-incrementing behaviour in these two systems respectively but that the effect of the regularisation is to lead to a progressive loss of the higher period orbits.

Key words. regularised discontinuous map, period-adding, period-incrementing, grazing bifurcation, corner-collision bifurcation, impact-oscillator, cam-follower system, border-collision bifurcation

AMS subject classifications. 34C23, 34K07, 37G15, 37G25, 37G35, 37M05, 70F35, 70K40, 70K50.

1. Introduction. Many problems in electronics [14] [15], and other applications which have discrete switching behaviour, for example neuron-firing models [16], can give rise to one-dimensional discontinuous piecewise-smooth maps. In the special case of piecewise-linear discontinuous maps these can be written in the generic form

$$x \mapsto F(x) \equiv \begin{cases} \lambda_1 x + \mu & \text{if } x - c < 0 \\ \lambda_2 x + \mu - l & \text{if } x - c \geq 0 \end{cases} \tag{1.1}$$

(where l can be scaled to equal ± 1). An example of a discontinuous piecewise-linear map, often referred to as a 'map with a gap' [14], is illustrated in Figure (1.1). The existence of the discontinuity at $x - c = 0$ and its interaction with the ω-limit sets of the dynamics in border-collision bifurcations gives rise to surprisingly rich dynamics. Jain and Banerjee [15] showed numerically the that this can lead to the creation of a very large number of periodic orbits and that the associated bifurcation diagrams for these orbits can be very complex with subtle transitions between the orbits, sudden jumps to chaos and the sudden destruction of invariant sets for maps of the form (1.1). Further analytical results for the dynamics of the one-dimensional discontinuous map are presented in the papers by Hogan et. al. [14] and Avrutin and Schanz [3] [4], with additional references in [16], [5], [7] and [10]. Key results include the existence of high period period orbits described by bifurcation diagrams with *period-adding* or *period-incrementing* sequences occuring as a parameter μ varies. Period-adding describes a situation where a period $n + m$ orbit arises for a parameter value between those for which two separate orbits of period n and m occur and is seen when $\lambda_1 > 0, \lambda_2 > 0$. We also see the period of the observed orbits described in terms of Farey-sequences and the winding number of the orbits behaving like Cantor functions. In contrast,

*Centre for Nonlinear Mechanics, Department of Mathematics, University of Bath, UK, BA2 7AY. (S.R.Pring@bath.ac.uk and C.J.Budd@bath.ac.uk)

†Corresponding author

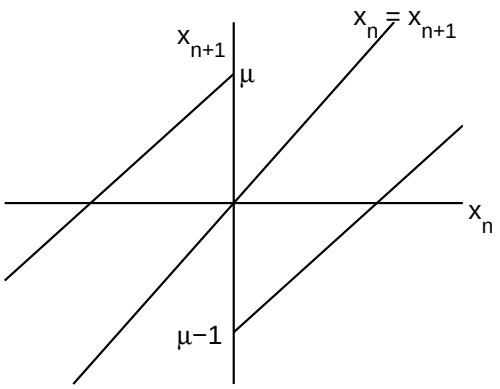

Fig. 1.1: A plot of the map (1.1) for parameters $\mu = 0.5, l = 1, \lambda_1 = 0.8, \lambda_2 = 0.8$ and $c = 0$.

period-incrementing describes a situation in which a period $n+1$ orbit follows from a period n orbit as μ is increased (or decreased) and this case arises when $\lambda_1\lambda_2 < 0$. The maps with $\lambda_1 > 0, \lambda_2 > 0$ and $\lambda_1\lambda_2 < 0$ will be referred to as *period-adding maps* and *period-incrementing maps* respectively, and we will give two examples of mechanical systems showing each type of behaviour.

In contrast to such one-dimensional discontinous maps, many piecewise-smooth dynamical systems, such as impact oscillators, cam-follower systems, friction oscillators or many of the systems studied in [10], have dynamics which can be studied exactly by using two-dimensional *continuous* maps. Such maps may themselves be non-smooth and have (for example) locally square-root behaviour. The analysis of such systems has generally been rather local in nature, for example we now have a fairly complete understanding of the dynamics of impact oscillators very close to a grazing bifurcation where the local square-root form of the map dominates. However, this analysis has often not considered the broader global behaviour of such oscillators. A purpose of this paper is to show that over a broad range of parameters, a good 'outer' approximation to such two-dimensional *continuous* maps is given by a regularised one-dimensional map with a gap and that the analysis of the dynamics of such maps gives very useful insights into the global dynamics of the more general (physical) system. In particular, in this paper we consider two mechanical systems which generate two-dimensional Poincaré maps which are closely approximated in a certain limit by regularised maps with gaps that can then in turn be approximated by maps of the form (1.1).

To make sense of the above, we shall refer to a *regularised discontinuous map* or a *regularised map with a gap* as a one-dimensional map which is continuous for all x but which varies very rapidly over a narrow interval of width proportional to $\epsilon \ll 1$ and that away from this interval it takes the form of (1.1). The regularised discontinuous maps which we study in this paper arise when we study *(i)* corner-collision impacts of a cam-follower system and *(ii)* the single-degree-of-freedom impact oscillator. The difference between this paper and other studies on the cam-follower and impact oscillator is that we take a global approach to deriving the stroboscopic map for each of

these systems rather than deriving the local nonlinear effects close to a discontinuity bifurcation.

In particular, for the cam-follower system we study the stroboscopic maps related to impacts of a cam follower with a rotating cam with a corner which is smooth but has very large curvature κ. We show that globally such stroboscopic maps can be closely approximated by one dimensional continuous maps, which vary rapidly over an interval inversely proportional to κ and which can, in turn be approximated by discontinous maps of the form (1.1) for which $\lambda_1 > 0, \lambda_2 > 0$ (leading to period-adding). For the impact oscillator we study the grazing dynamics associated with large dissipation systems for which, under a change in parameters, a non-impacting orbit (which has *linear* dynamics) evolves to an orbit with a high-velocity impact (which we also show has close to linear dynamics) via a grazing impact. Very close to the grazing impact it is known [18] that the (two-dimensional) stroboscopic map for this system is locally of square-root form. However, we will show that away from this local region the outer form of the map is closely approximated by (1.1) with $\lambda_1\lambda_2 < 0$ (leading to period-incrementing). In this case the local effects of the rapid change in the square-root terms in the map (including the locally infinite gradient) are well approximated by the discontinuity in the map (1.1) giving an outer linear approximation of the stroboscopic map.

We show that the bifurcation diagrams of the dynamics of the two mechanical systems can be understood by studying the bifurcation diagrams of the two cases of the discontinuous maps (1.1) resulting in respectively period-adding or period-incrementing behaviour. We also consider carefully the effects of increasing the regularisation parameter ϵ from zero and obtain estimates in terms of ϵ for the regions of existence of the period-N orbits. We show that an increase in ϵ leads to a progressive loss of existence of the higher period orbits, which are replaced by intervals of chaotic behaviour.

The layout of the remainder of this paper is as follows. In §2 we introduce and then study the dynamics of the two mechanical systems described above. In §3.1 and §3.2 we derive the stroboscopic map and the approximate one-dimensional regularised discontinuous map for the cam-follower and impact oscillator systems respectively. In §4 we study the regularised discontinuous map obtained for the cam-follower system (leading to period-adding) and in §5 we study the regularised discontinuous map which is obtained when we consider an alternative approach to deriving the stroboscopic map for the impact oscillator (leading to period-incrementing).

2. Two examples of mechanical systems leading to regularised maps with gaps. In this section we consider in more detail the two mechanical systems that we will study, namely the cam-follower and the damped impact oscillator near grazing. We demonstrate numerically that the Poincaré map for each system takes the form of a regularised map with a gap and that the two cases lead to period-adding and period-incrementing type maps respectively. In each case we give the computed bifurcation diagram for each mechanical system and these will be compared in §4 and §5 with the corresponding bifurcation diagrams for the associated maps.

2.1. Example 1 - The Cam-follower system. The cam-follower system is used in many mechanical applications, most notably in internal combustion engines. It is an example of a system where impacts take place and comprises of a follower, which can move in the vertical direction only, lying on top of and impacting with a

cam rotating at a fixed angular velocity ω about a fixed axis. The shape of the cam at time t is described in radial coordinates (r, θ) by the 2π periodic function

$$r = G(\theta - \omega t). \tag{2.1}$$

The height of the cam (defined to arise when $\theta = 0$) is given by the periodic function

$$g(t) \equiv G(-\omega t)$$

with period $T = 2\pi/\omega$. The follower is assumed to have location $u(t)$ and to initially lie on top of (and be in contact with) the rotating cam so that $u(t) = g(t)$; however, the follower and cam can lose contact at sufficiently high enough rotation speeds ω so that $u(t) > g(t)$ for a interval of time until it comes back into contact. At contact the follower impacts with the cam and repeated impacts are expected to occur at later times. To model this system we assume that when out of contact with the cam the follower has its motion governed by the ordinary differential equation

$$\frac{d^2u}{dt^2} + \alpha\frac{du}{dt} + u = 0 \quad \text{for} \quad u(t) > g(t). \tag{2.2}$$

An impact then occurs when $u(t) = g(t)$ and we assume this to be instantaneous and modelled by the impact restitution law

$$\tilde{v}^+ = -r\tilde{v}^-, \tag{2.3}$$

where $\tilde{v} = du/dt - dg/dt$ is the relative velocity of the follower with respect to the cam and $\tilde{v}^-$ and $\tilde{v}^+$ are the relative velocities immediately before and after impact respectively.

di Bernardo et al. [1] [21] have studied certain aspects of the dynamics of such systems and it has been shown that 'corners' in the cam, which are defined to be those points at which the function $G(\phi)$ loses smoothness in some manner, can have a significant effect on the dynamics of the follower when impacts occur close to the corners. The paper [21] studied the case when the 'corner' was a discontinuity in the second-derivative of the cam-profile so that the function $g(\theta)$ had a continuous first derivative but contained a small finite number of points at which it had a discontinuity in the second derivative. In [21] an analysis was carried out of the resulting stroboscopic map related to the impact dynamics. This was shown to be piecewise-linear continuous and an analysis based on Feigin's theory [11] of such can then be applied to determine the resulting dynamics of the follower system.

In this paper we consider the profile of the cam G to either have discontinuous first derivative at a discrete set of values of θ^*, such as a square cam, or for which the derivative of the function G changes very rapidly in a small neighbourhood of θ^*, such as a square cam with corners with high curvature. The curvature of the smoothed corners which we consider is $\kappa(t^*) = \eta^2/\delta$ with $0 < \delta \ll 1$, see the form of $g(t)$ below. In contrast to the earlier analysis of [21], we will show that the dynamics of orbits in the case where the follower impacts close to the (smoothed) corner is described by a stroboscopic map which takes the form of a (regularised) one-dimensional map with a gap. This is profoundly different from dynamics of the systems described by a continuous map.

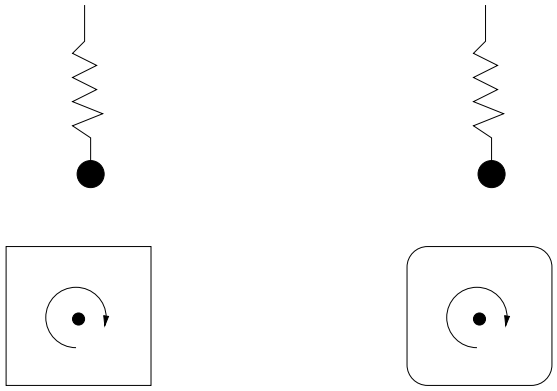

Fig. 2.1: A square-cam and a square-cam with smoothed corners, the follower is represented by a mass attached to a damped spring.

For a square-cam, see Figure (2.1a), the height of the cam $g(t)$ is given by the function

$$g(t) = d + \frac{\beta}{\cos(\omega\hat{t}) + \sin(\omega\hat{t})} \text{ with } \hat{t} = \mod\left(t + \tfrac{\pi}{4\omega}, 2\pi\right) \tag{2.4}$$

and a plot of the cam-profile $g(t)$ and the impacting follower is given in Figure (2.2). The corners of the cam occur at values of time equal to $\frac{\pi}{2} + \frac{n\pi}{2\omega}$ for $n \in \mathbb{N}$ and impacts

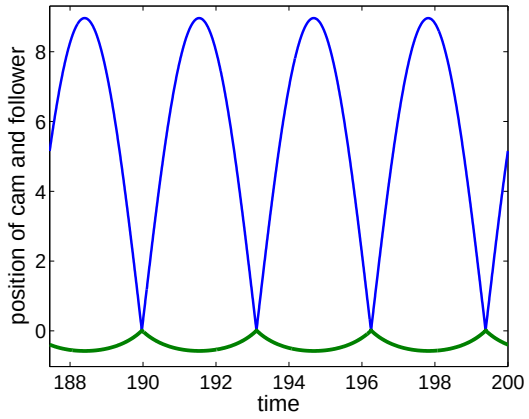

Fig. 2.2: A plot of the follower periodically impacting the cam for the system (2.2)-(2.3) with $g(t)$ given by equation (2.4) with parameter values $\omega = 0.5002, d = -1.99, \beta = 2, \alpha = 0$ and $r = 0.8$.

occur local to these corners. If we now smooth out the corners of the square-cam and assume that a corner of the cam exists at times $t = t^*$ then locally about $t = t^*$ we approximate the cam profile $g(t)$ by the function

$$g(t) = h - \frac{\eta^2(t - t^*)^2}{2\delta} \quad \text{if} \quad |t - t^*| < \delta/\eta \tag{2.5}$$

and

$$g(t) = \begin{cases} \eta(t-t^*) + h + \frac{\delta}{2} & \text{if } t < t^* - \delta/\eta \\ -\eta(t-t^*) + h + \frac{\delta}{2} & \text{if } t > t^* + \delta/\eta. \end{cases} \tag{2.6}$$

This local approximation of the corner corresponds to the square-cam profile (2.4) provided $h = d + \alpha$ and $\eta = \alpha\omega$.

In this paper we study the interesting dynamics which occurs when impacts between the follower and the cam occur repeatedly close to the corners and in Figure (2.2) we have plotted an example of an orbit with precisely this property. An analysis of the motion of the follower can be obtained by considering a stroboscopic map P and we assume that a single impact occurs between the Poincaré surfaces of the stroboscopic map. The time period that we sample over is the interval $[\frac{n\pi}{2\omega}, \frac{(n+1)\pi}{2\omega})$ and if we let $T = \frac{\pi}{2\omega}$ then the stroboscopic map is

$$P : (u(nT), v(nT)) \to (u(n+1)T, v((n+1)T)), \quad n = 0, 1, 2, \ldots \tag{2.7}$$

where $u(nT)$ and $v(nT)$ denote the position and velocity of the follower at time $t = nT = n\pi/2\omega$. To construct such a map P we have to determine the trajectory of the follower before it hits the cam, the impact with the cam, and the subsequent trajectory. Of particular interest in this paper is the form that this map takes when the resulting trajectory impacts with the cam close to a corner in the cam profile $g(t)$ at times $t = nT + T/2$. For simplicity, we assume that during each sampling period $[nT, (n+1)T]$ only one such impact occurs and such behaviour will occur when the follower starts well above the cam and the time at which the follower impacts the cam is close to $nT + T/2$. If $v(nT)$ is close to zero and α is also small then the free motion of the follower is given approximately by $u(t) = u(nT)\cos(t - nT)$ if

$$h \ll 1 \quad \text{and} \quad \omega \approx \frac{1}{2}.$$

This implies that at $t = nT+T/2 \approx \frac{n\pi}{2\omega}+\pi/2$ the position of the follower $u(nT+T/2) \approx h$ and the height of the cam is at $t = nT + T/2$ is $g(nT + T/2) = h$. Therefore, it is for such values that we expect to see the trajectory impacting close to the corner and we study the stroboscopic map P. A numerical plot of the image $(u(T), v(T))$ of the resulting stroboscopic map P, taking fixed $v(0) = -0.005$ and varying $u(0)$, is given in Figure (2.3). This figure displays a number of key features of the map. Firstly, we see that whilst the map is continuous there is a sharp transition in its form around the point $u(0) \equiv u_c \approx 19$ where u_c corresponds to the initial value of position which leads to an impact at the corner at time $T/2$. Trajectories which have initial position either side of u_c impact either side of the corner and this leads to the sharp change in the form of the stroboscopic map. The second observation that we make is that away from orbits which impact close to the corner, the stroboscopic map is very closely approximated by a piecewise-linear map with a gap of the form (1.1) with $\lambda_1 \approx \lambda_2 > 0$. Indeed, an approximation for this stroboscopic map is derived in §3.1 and we show that a regularised discontinuous map is a good approximation to this stroboscopic map. In Figure (2.3) we overlay the following discontinuous piecewise-linear approximation

$$u_{n+1} = \begin{cases} ru_n + \eta(1+r) & \text{if } u_n < u_c \\ ru_n - \eta(1+r) & \text{if } u_n \geq u_c. \end{cases}$$

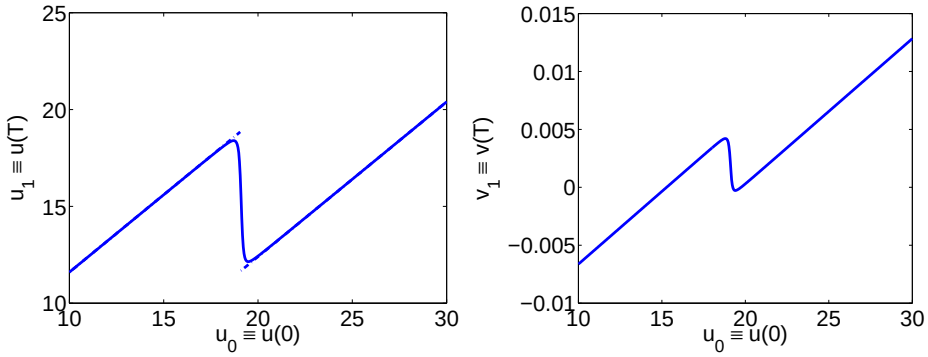

(a) (b)

Fig. 2.3: The stroboscopic map for a smoothed corner cam system given by equations (2.2)-(2.3) with $g(t)$ given by equations (2.5) and (2.6) with constant initial velocity $v(0) = -0.005$ and initial position $10 \leq u(0) \leq 30$. The parameters are $\omega = 2.001, r = 0.8, h = 0.01, \eta = 2$ and $\delta = 10^{-5}$. The discontinuous piecewise-linear approximation is shown by the dashed line in the left-hand figure.

A derivation of this map is given in §3.1 and the regularised version of this map is given in equation (3.2) and a normal-form version in equation (3.3). We note that the discontinuous piecewise-linear approximation, which is denoted by the dashed-lines in Figure (2.3), agrees well with the numerically obtained map for a large set of initial values.

A bifurcation diagram for the cam-follower system is given in Figure (2.4) in which we plot the ω-limit sets of the system for a range of values of the maximum height h of the cam. We can see a number of important features in this diagram which are quite different from that obtained by di Bernardo et. al. [21] for the smoother cam profile which they study. In particular a period-1 orbit which is stable for $h > 0.013$ dramatically loses stability as h decreases and trajectories intersect the corner of the cam. At $h \approx 0.013$ a very large number of periodic orbits are created and as h decreases the period of these orbits decreases monotonically in general. However, we also see intervals of *period-adding* where higher period orbits of period $n_1 + n_2$ exist for values of the parameter h which lie between between the intervals of existence for orbits of (lower) periods n_1 and n_2 of lower period and are in fact are a concatenation of these periodic orbits. As an example, in Figure (2.4) we see at $h \approx 0.0095$ a period-11 orbit which lies between a period-5 orbit arising when $h \approx 0.009$ and a period-6 orbit when $h \approx 0.006$. Close to the higher periodic orbits we also see evidence of chaotic behaviour. Such behaviour, as we shall see later, is exactly that expected from a corresponding regularised one-dimensional map with a gap, see equations (3.2) and (3.3).

2.2. Example 2: The impact oscillator. The single-degree-of-freedom impact oscillator has received much attention in the nonsmooth literature due to its rich dynamics and references include [9] [17] [18] [19]. For completeness, we give a short description of the impact oscillator here and more details can be found in [10]. We consider a particle which has position $u(t)$ and assume that if $u(t) > 0$ the particle

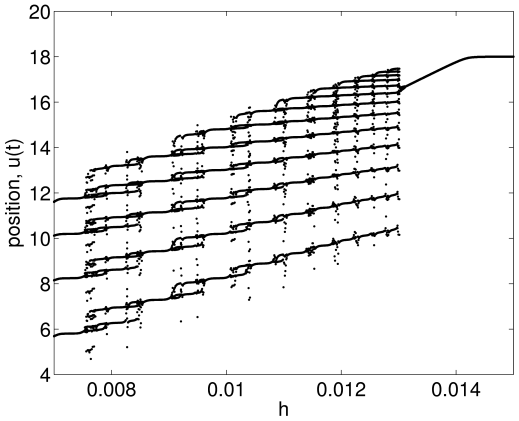

Fig. 2.4: The bifurcation diagram for the cam-follower system (2.2)-(2.3) with smoothed corners given by height profile equations (2.5) and (2.6) where the parameters are $\eta = 2$, $\omega = 0.501$, $\alpha = 0$, $r = 0.8$ and $\delta = 10^{-5}$. The curvature at a corner is $\kappa = 8 \times 10^4$. Note the existence of period-adding behaviour of the periodic orbits.

moves under the action of a smooth, parameterised, periodic forcing function $f(t)$ in a damped system which is described by the second-order differential equation

$$\frac{d^2u}{dt^2} + \alpha\frac{du}{dt} + u = f(t) \quad \text{if } u(t) > 0. \tag{2.8}$$

In contrast to the cam-follower system we will be considering the case of moderately large values of the damping coefficient α. When $u(t) = 0$ we assume an impact occurs with an impact wall and that the particle instantaneously changes direction. As in the case of the cam-follower system, we model this using the restitution law

$$v^+ = -rv^- \quad \text{if } u(t) = 0, \tag{2.9}$$

with $0 < r < 1$ and v^- and v^+ denoting the particle velocity immediately before and after impact. To analyse the system (2.8) and (2.9), which is commonly referred to as the impact oscillator system, we construct a strobscopic map which maps the flow from a suitable Poincaré surface in phase space back to itself. However, we restrict our attention to the specific *smooth* forcing function

$$f(t; \omega, d, t_0) = d + \cos(\omega(t + t_0)) \tag{2.10}$$

which has period $T = 2\pi/\omega$ but the analysis in this paper is applicable to any smooth periodic forcing function $f(t)$. As for the cam-follower system, a suitable Poincaré surface samples the position $u(t)$ and velocity $du/dt = v(t)$ at times $t = 0, T, 2T, 3T \ldots$. A numerically calculated image$(u(T), v(T))$ of the stroboscopic map is denoted by the solid line in Figure (2.5) for the case of $u(0) \equiv u_0$ *fixed* and with $v(0) \equiv v_0$ *varying* and fixed parameters $\alpha = 3, \omega = 2.1, r = 0.8, d = 0.08$ and $t_0 = 2.1$. In this figure we have plotted the stroboscopic map for a large range of initial impact velocities and if $v_0 > -0.1868$ no impact occurs and if $v_0 < -0.1868$ one impact occurs in the time

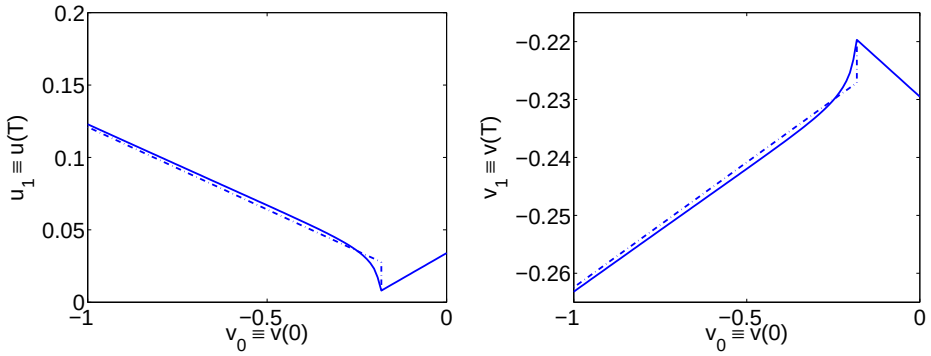

(a) (b)

Fig. 2.5: The solid line denotes the stroboscopic map for the impact oscillator system (2.8)-(2.10) for parameter values $\alpha = 3, \omega = 2.1, r = 0.8, d = 0.08$ and $t_0 = 2.1$ with initial position $u_0 = 0.04$. The dash-dot line denotes the linear approximation of the stroboscopic map, see (3.10) and (3.11). The grazing orbit occurs at $v_g \equiv v_0 = -0.1868$ when $u_0 = 0.04$.

interval $[0, T]$. Figure (2.5) displays a number of key features of the stroboscopic map for an impact oscillator and for $v_0 < -0.4$ or for $v_0 > -0.1868$ the map is very close to being linear, although with different signs for the slope. For $-0.4 < v_0 < -0.1868$ the stroboscopic map has a short region over which it takes a (well-known) square-root form due to a grazing (zero velocity) impact when $v_0 = -0.1868$. The conventional analysis of the impact oscillator [6] [12] [17] [18] [19] [20] involves considering the local dynamics of impacting orbits close to this transition point, known as the grazing bifurcation. However, we can see immediately from Figure (2.5) that the global form of the stroboscopic map is close to that of a map with a gap with the square-root part of the map acting as a smooth regularisation of the discontinuity. Indeed a piecewise-linear discontinuous approximation to the stroboscop map is given in Figure (2.5) and it is denoted by a dashed line. The piecewise-linear discontinuous approximation which we have plotted is

$$\begin{pmatrix} u_{n+1} \\ v_{n+1} \end{pmatrix} = \begin{cases} D \begin{pmatrix} u_n \\ v_n \end{pmatrix} + \mathbf{g} & \text{for } v_0 > v_g \text{ (non-impacting orbits)} \\ -rD \begin{pmatrix} u_n \\ v_n \end{pmatrix} + \mathbf{g} & \text{for } v_0 \leq v_g \text{ (impacting orbits)} \end{cases}$$

where v_g denotes the initial velocity at which a grazing bifurcation occurs. The matrix D and the vector $\mathbf{g}$ are defined in §3.2 by equation (3.7). In the next section we make the derivation of this map more precise by considering a regularisation of this map and show that for the values of α considered, i.e. large values of α corresponding to heavy damping, the dynamics of the system are well described by a regularised one-dimensional map with a gap.

A bifurcation diagram for the impact oscillator when the parameter d of the forcing function $f(t)$ in equation (2.10) is varied is plotted in Figure (2.6) with the vertical coordinate denoting the position of the impact oscillator at periodic intervals of time T. The effect of varying parameter d is to bring the impact oscillator closer to the

impacting wall at position $u = 0$. If d is sufficiently large enough i.e. the impact oscillator is sufficiently far enough away from the impact wall, and α the damping parameter is large enough then no impacts occur. This behaviour can be seen in Figure (2.6) where for $d > 0.14$ a non-impacting period-1 orbit exists and as d passes through $d = 0.14$ (approximately) a grazing bifurcation occurs. The result of which is the generation of a number of impacting periodic orbits and as d is decreased a reverse *period-incrementing* sequence exists with the period of the orbits decreasing monotonically by one as d decreases. Unlike the case of the cam-follower, we do not see windows of higher periodicity and the periodic orbits overlap rather than concatenate and for $d \approx 0.095$ we see coexistence of orbits of periods one and two. In §4 we compare the bifurcation diagram generated by the regularised discontinuous map with Figure (2.6) which is computed directly from simulations of the impact oscillator.

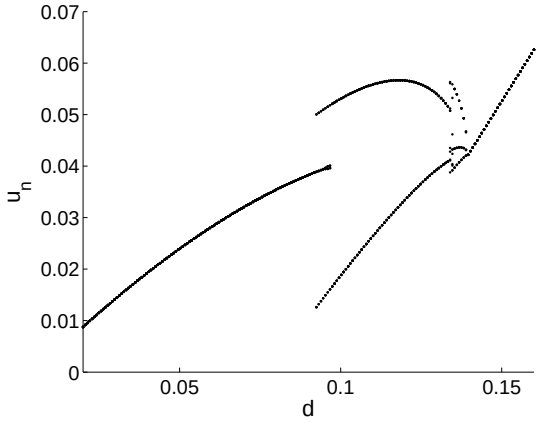

Fig. 2.6: The bifurcation diagram for the impact oscillator (2.8)-(2.10) with parameters $\omega = 2.1, r = 0.8, t_0 = 2.1$ and $\alpha = 3$. The vertical coordinate is a nonlinear coordinate transformation of the position u_n and velocity v_n at times $t = nT$, this is discussed in §3.2.4.

3. Derivation of regularised discontinuous maps for the mechanical systems. In sections §3.1 and §3.2 we look at the two mechanical examples in more detail and show how the stroboscopic map of each can be approximated by a regularised map with a gap, which has period-adding form for the cam-follower and period-incrementing form for the impact oscillator.

3.1. Stroboscopic map for the cam-follower system. We firstly derive a stroboscopic map which describes the dynamics of the cam-follower system as illustrated in Figure (2.2) and we aim to approximate the stroboscopic map by a one-dimensional regularised discontinuous map. As discussed in §2, we consider a stroboscopic map P which evolves the position $u(t)$ and velocity $v(t)$ of the follower from time $t = nT$ to time $t = (n+1)T$. We can, without loss of generality, restrict our attention to the time interval $[0, T]$ and let $(u_0, v_0) = (u(0), v(0))$ and $(u_1, v_1) = (u(T), v(T))$ such that the stroboscopic map we consider is $(u_0, v_0) \mapsto (u_1, v_1)$. Our interest is the form of the stroboscopic maps for which the trajectory impacts close to the corner of

the function $g(t)$ which arise for example if $\omega \approx 0.5$ and $h, \alpha, v_0 \approx 0$.

We firstly consider the general form of a stroboscopic map and to construct it we consider a trajectory starting from (u_0, v_0) and assume that this impacts close to the corner at some time $t_i \approx T/2$. The trajectory will then rebound and we can determine (u_1, v_1) by evaluating the flow following the rebound. In Figure 3.1 we illustrate this by plotting two trajectories, one of which impacts *before* the corner and the other of which impacts *after* the corner. To ensure that such impacts occur we require that

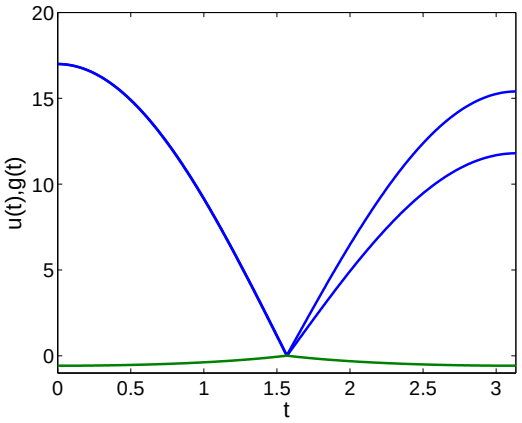

Fig. 3.1: Two trajectories which impact either side of a corner of the cam-follower system (2.2)-(2.3) with the height profile of the cam given by function (2.4). The parameters for the cam-follower system are $\omega = 0.501, r = 0.8, d = -1.99, \alpha = 0, \beta = 1$ and the initial position in both trajectories is $u(0) = 17$ and the initial velocities are $v(0) = -0.06$ and $v(0) = -0.01$.

the orbits intersect the surface $g(t)$ *transversally* close to the corner, this implies that $v(t) < dg/dt$ just before the impact. This condition prevents the occurrence of grazing impacts with zero relative velocity. It then follows from the results in [10] Chapter 2 that *the smoothness of the map P is at least as good as that of the function $g(t)$*. Thus in this case we guarantee that overall P is continuous in its arguments and also has continuous first derivatives. If $v_0 \approx 0$, $\alpha \approx 0$ and $\omega \approx 0.5$, then as $u \approx u_0 \cos(t)$ we have $u(T/2) \approx 0$ and $v(T/2) \approx -u_0$. As $-\eta < dg/dt < \eta$ then a transverse impact close to the corner is guaranteed provided that $u_0 > \eta$. We shall insist on this condition which also guarantees that there will be no further impacts with $g(t)$ for t close to $T/2$.

The corner impact we consider has close similarities with the corner impact studied in [7] and we can make use of the two-dimensional stroboscopic maps derived in paper [7]. If we let t_i denote the time at which an impact occurs then we have the condition $u(t_i) = g(t_i)$ and we consider impacts such that t_i is close to $T/2$. If $t_i < t^- \equiv T/2 - \delta/\eta$ or $t_i > t^+ \equiv T/2 + \delta/\eta$ then the follower impacts the linearly approximated region of $g(t)$ which takes the form of an inverted V. A similar situation to this was studied in [7] which considered the impacts of a trajectory with a surface of exact V-shape arising in a multi-component collision. It was shown in [7] that if v_0 is small, then provided ω is close to $1/2$ that v_1 is also small (as are subsequent

iterates v_n) and the map from u_0 to u_1 is (to leading order) one-dimensional. To derive this map we set v_0 equal to zero and consider the map u_0 to u_1. Following [7], this is given as

$$u_1 = ru_0 + \eta(1+r) \text{ if } t_i < t^-, \qquad u_1 = ru_0 - \eta(1+r) \text{ for } t_i > t^+. \tag{3.1}$$

We note that the first derivative of both maps depends on the restitution coefficient r and not on the gradient $\pm\eta$ of the linear sections of the cam-profile. Note also that this map takes the form of (1.1) with $\lambda_1 = \lambda_2 = r$. It is hence of the general form of a period-incrementing map with a gap. As u_0 is increased the time of impact t_i also increases so that (at least locally) if $u_0 < u_\alpha$, $t < t^-$, and if $u > u_\gamma$ then $t > t^+$. Indeed

$$u_\alpha = (h - \delta/2)/\cos(T/2 - \delta/\eta) \quad \text{and} \quad u_\gamma = (h - \delta/2)/\cos(T/2 + \delta/\eta).$$

Observe that in general $u_\gamma - u_\alpha = \mathcal{O}(\delta)$. Intermediate to these two values is the point $u_0 = u_c$ such that if $u_0 = u_c$ then $t_i = T/2$ and $u_c = h/\cos(T/2)$. If the corner is not smoothed then $u_\alpha = u_c = u_\gamma$ and the map from u_0 to u_1 has a discontinuity of size $-2\eta(1+r)$.

We now consider the case of a square-cam with smoothed corners such that $\delta > 0$. To derive an approximation to the stroboscopic map for the interval $u_\alpha < u_0 < u_\gamma$, we use the previous result that such a map must be globally C^1 and in this interval of width δ, where the trajectory impacts with the smooth corner of the cam, the map itself will be smooth. Rather than attempting to derive a precise form for the map, it is thus reasonable to use a smooth spline to approximate it, enforcing continuity of first derivatives at the points u_α and u_γ. The simplest such spline with sufficient degrees of freedom to do this is a Hermite cubic interpolant. However, it is somewhat easier to analyse a continously differentiable piecewise quadratic spline approximation and we do this in §5. Accordingly, if we set $u_\beta = (u_\alpha + u_\gamma)/2$ then this takes the form

$$u_1 = \begin{cases} ru_0 + \eta(1+r) & \text{if } u_0 < u_\alpha \\ \frac{-\eta(1+r)}{(u_\beta - u_\alpha)^2}(u_0 - u_\beta)^2 + \left(r - \frac{2\eta(1+r)}{(u_\beta - u_\alpha)}\right)(u_0 - u_\beta) + ru_\beta & \text{if } u_\alpha < u_0 < u_\beta \\ \frac{\eta(1+r)}{(u_\beta - u_\gamma)^2}(u_0 - u_\beta)^2 + \left(r - \frac{2\eta(1+r)}{(u_\gamma - u_\beta)}\right)(u_0 - u_\beta) + ru_\beta & \text{if } u_\beta < u_0 < u_\gamma \\ ru_0 - \eta(1+r) & \text{if } u_\gamma < u_0. \end{cases} \tag{3.2}$$

A plot of this map and the numerically obtained stroboscopic map is given in Figure (3.2) and we can see that there is reasonably good comparison between the two.
To further simplify the map and reduce the number of parameters of map (3.2), we put the map (3.2) into standard form by a change of variable

$$x_n = (u_n - u_\beta)/(2\eta(1+r))$$

and letting

$$\lambda = r, \quad \epsilon = (u_\beta - u_\alpha)/(2\eta(1+r)), \quad \mu = ((r-1)u_c + \eta(1+r))/(2\eta(1+r))$$

and noting that approximately $u_\gamma - u_\beta = u_\beta - u_\alpha$. Considering the map over the general time interval $[nT, (n+1)T]$ gives the regularised discontinuous map which approximates the cam-follower system as

$$x_{n+1} \equiv F(x_n) = \begin{cases} f_1(x_n) = \lambda x_n + \mu & \text{if } x_n < -\epsilon \\ f_2(x_n) = \frac{-1}{2\epsilon^2}x_n^2 + (\lambda - \frac{1}{\epsilon})x_n + \mu - \frac{1}{2} & \text{if } -\epsilon < x_n < 0 \\ f_3(x_n) = \frac{1}{2\epsilon^2}x_n^2 + (\lambda - \frac{1}{\epsilon})x_n + \mu - \frac{1}{2} & \text{if } 0 < x_n < \epsilon \\ f_4(x_n) = \lambda x_n + \mu - 1 & \text{if } x_n > \epsilon. \end{cases} \tag{3.3}$$

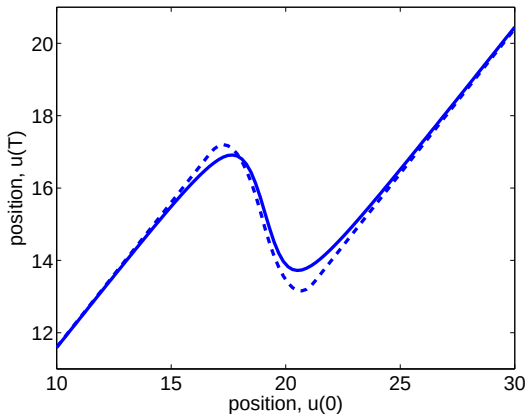

Fig. 3.2: The dashed line denotes the piecewise-quadratic map (3.2) and the solid line is the numerical solution of the cam-follower system (2.2)-(2.3) with cam profile $g(t)$ given by (2.5) and (2.6). The parameters are $\omega = 0.501, \eta = 2, r = 0.8, h = 0.01$ and $\delta = 10^{-4}$ and the initial velocity is $v_0 = -0.005$. Note in this figure δ is $\delta = 10^{-5}$ whereas in Figure (2.3a) it is $\delta = 10^{-4}$.

A plot of map (3.3) is given in Figure (3.3). We study the bifurcation diagrams and

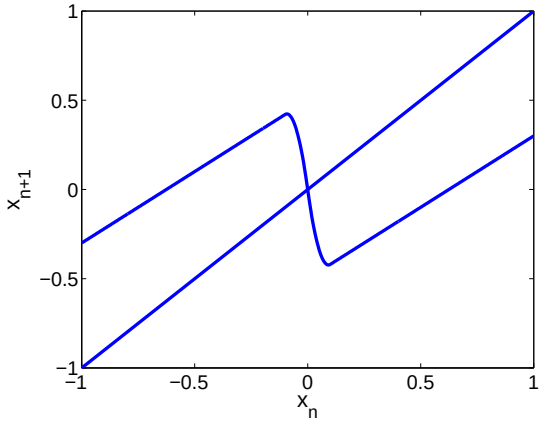

Fig. 3.3: A plot of the map (3.3) for parameters $\lambda = 0.8, \mu = 0.5$ and $\epsilon = 0.1$.

dynamics of the period-adding type of regularied map with a gap (3.3) in §4.

3.2. The impact oscillator. In this section we present a method for deriving the global form of the stroboscopic map for the impact oscillator which considers the linear dynamics either side of a grazing bifurcation and we show that this takes the form of a period-incrementing regularised map with a gap. This calculation complements the derivation of the local nonlinear discontinuity map for low velocity impacts close to a grazing bifurcation and the resulting local nonlinear stroboscopic map which

can be found in [10]. Our method considers the outer *linear* dynamics of the impact oscillator which is illustrated in Figure (2.5) where we can see that the stroboscopic map is globally piecewise-linear for a sufficiently large set of initial conditions with a small region of initial values where the map takes a square-root form.

To derive the global form of the stroboscopic map we consider the position $u(t)$ and velocity $v(t)$ of the system (2.8)-(2.10) at times $t = 0, T, 2T, 3T, \ldots$ with $T = 2\pi/\omega$ (this is identical to the cam-follower system). Again, without loss of generality, we consider the dynamics over the time interval $[0, T]$ and we introduce a state vector $\boldsymbol{w}(t) = (u(t), v(t))$ and let $\boldsymbol{w}_0 = (u(0), v(0)) \equiv (u_0, v_0)$ denote the position and velocity at time $t = 0$ and let $\boldsymbol{w}_1 = (u(T), v(T)) \equiv (u_1, v_1)$ denote the position and velocity at time $t = T$. We shall only consider the stroboscopic map for orbits which impact once or not at all during the time period $[0, T]$ and will consider the effects of varying the initial conditions along a set transverse to that set of initial conditions which leads to a grazing impact at a time t_i at which u and v both vanish. We firstly state the stroboscopic map $\boldsymbol{w}_0 \mapsto \boldsymbol{w}_1$ for those orbits which do not impact in this time interval.

3.2.1. Non-impacting orbits. The dynamics of the particle when it is out of contact with the impact wall is given by equation (2.8) and using the state vector $\boldsymbol{w}(t)$, equation (2.8) can be re-written as

$$\dot{\boldsymbol{w}} = B\boldsymbol{w} + \boldsymbol{c} \tag{3.4}$$

where matrix B and vector $\boldsymbol{c}$ are defined as

$$B = \begin{pmatrix} 0 & 1 \\ -1 & -\alpha \end{pmatrix} \quad \text{and} \quad \boldsymbol{c} = \begin{pmatrix} 0 \\ f(t;\omega,h,t_0) \end{pmatrix} \equiv \begin{pmatrix} 0 \\ h + \cos(\omega(t+t_0)) \end{pmatrix}.$$

The solution of equation (3.4) is simply

$$\boldsymbol{w}(t) \equiv \Phi(\boldsymbol{w}_0, t) = e^{Bt}\boldsymbol{w}_0 + e^{Bt}\int_0^t e^{-Bs}\boldsymbol{c}ds; \tag{3.5}$$

therefore, the stroboscopic map $\boldsymbol{w}_0$ to $\boldsymbol{w}_1$ for a non-impacting orbit is

$$P_T : \boldsymbol{w}_0 \mapsto \boldsymbol{w}_1 = D\boldsymbol{w}_0 + \boldsymbol{g} \tag{3.6}$$

where matrix D and vector $\boldsymbol{g}$ are defined as

$$D \equiv \begin{bmatrix} a & b \\ c & d \end{bmatrix} = e^{BT} \quad \text{and} \quad \boldsymbol{g} \equiv \begin{pmatrix} g_1 \\ g_2 \end{pmatrix} = e^{BT}\int_0^T e^{-Bs}\boldsymbol{c}ds. \tag{3.7}$$

Later we compose P_T with a *linear* zero-time discontinuity map to derive the stroboscopic map for an orbit with one high-velocity impact during the time interval $[0, T]$.

3.2.2. The grazing set. Having considered a trajectory which does not impact, we now vary a parameter, such as the initial velocity $v_0 \equiv v(0)$, until a first *grazing impact* occurs. A grazing impact is defined as a trajectory which impacts with zero velocity and the trajectory satisfies $u(t_g) = v(t_g) = 0$ for $t_g \geq 0$ and the set of initial conditions at $t = 0$, which leads to a grazing trajectory, is known as a *grazing set*. We denote the grazing set by $\mathcal{G}$ and it is defined as

$$\mathcal{G} = \{(u, v) | u(t_g) = v(t_g) = 0 \text{ with } 0 \leq t_g < T\}.$$

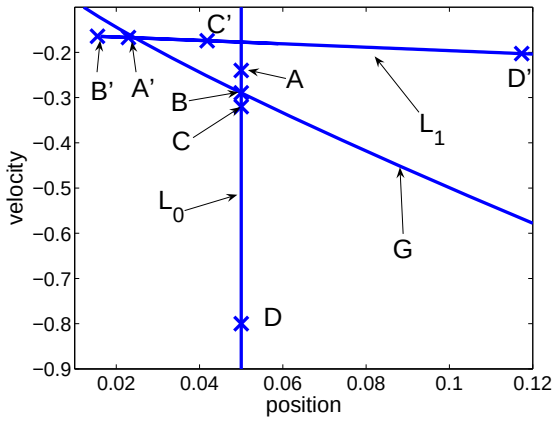

Fig. 3.4: The grazing set $\mathcal{G}$, a set of initial values L_0 and a final set of values L_1 after time T is plotted for parameters $\alpha = 3, \omega = 2.2, r = 0.8$ and $h = 0.13$ for the system (2.8)-(2.10). The initial values and their final positions for the trajectories A, B, C and D are denoted by $\times$.

An example of the grazing set $\mathcal{G}$ is plotted in Figure (3.4) and the grazing set separates impacting and non-impacting orbits. In Figure (3.4) we have also considered what happens to a set of initial conditions L_0 which crosses the grazing set $\mathcal{G}$. The set L_1 is the set of values after integrating the impact oscillator system with initial values L_0 forward for an amount of time $T = 2\pi/\omega$ (i.e. $L_0 \overset{T}{\mapsto} L_1$) and both L_0 and L_1 lie on the Poincaré surface. We also consider the dynamics of four initial values of the set L_0 and these four orbits are denoted by A, B, C and D and their initial trajectories are plotted in Figure (3.5). Trajectory B is a grazing trajectory, trajectory A is a non-impacting orbit and C and D are impacting trajectories (but with different impact velocities). The position of orbits $A - D$ after time T are denoted by $A' - D'$ and are elements of the set L_1. From Figure (2.5) we can infer that initial values of L_0 which lie between points A and B and also between points C and D are mapped *linearly* to L_1. Clearly points between A and B are mapped linearly because no impact has occured but orbits with initial conditions which lie between C and D impact with sufficiently high velocity that the stroboscopic map is linear for these initial conditions, this is clearly seen in Figure (2.5). Initial values which lie between points B and C are mapped *nonlinearly* by the stroboscopic map and these points are stretched far apart due to a square-root term in the locally derived stroboscopic map [18]. The set L_1 is folded onto itself with the value B', which corresponds to the grazing trajectory, lying at the cusp of the fold. A thorough study of the grazing set can be found in [8].

3.2.3. Impacting orbits and discontinuity map. We now consider the stroboscopic map for impacting orbits and we shall use the zero-time discontinuity mapping technique which is described in [10] to construct the stroboscopic map for high-velocity impacts which are modelled by a linear stroboscopic map. We denote the zero-time discontinuity map by P_{ZDM} and the stroboscopic map for an impacting orbit is given by $\boldsymbol{w}_1 = P_T \circ P_{ZDM}(\boldsymbol{w}_0)$. The difference to the usual study of the impact oscillator is that we consider a *linear* discontinuity map rather than a nonlinear disconitinuity map. The zero-time discontinuity map for low-velocity impacting

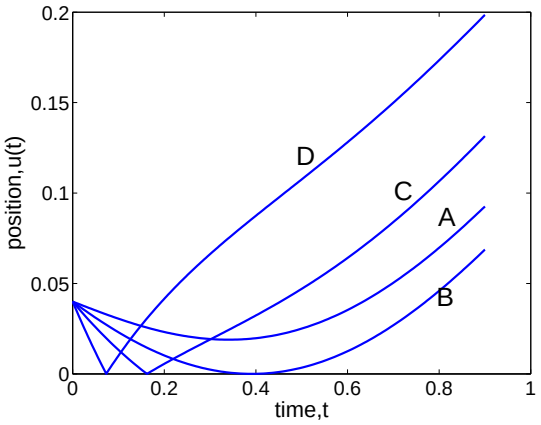

Fig. 3.5: Trajectories of the impact system (2.8)-(2.10) for parameters $\alpha = 3, \omega = 2.1, r = 0.8$ and $h = 0.08$. All trajectories have initial position $u(0) = 0.04$ and initial velocities $v(0)$, -0.1(A)(no impact), -0.1868(B)(grazing value), -0.3(C) and -0.6(D).

orbits, i.e. orbits which occur close to the grazing bifurcation, is derived in [10] and the map takes a square-root form which is, to lowest order,

$$P_{ZDM} : \begin{pmatrix} u_0 \\ v_0 \end{pmatrix} \mapsto \begin{pmatrix} u_0 \\ v_0 + (1+r)\sqrt{v_0^2 - 2A_0u_0} \end{pmatrix}. \tag{3.8}$$

This discontinuity map describes the dynamics of low-velocity impacting orbits remarkably well but we have seen in Figure (2.5) that the stroboscopic map for high-velocity impacts takes a linear form and we would like to derive a map which captures both the linearity and the global behaviour of the impact oscillator. The discontinuity map stated above is a lowest order approximation of the discontinuity map but a slightly higher order approximation is

$$P_{ZDM} : \begin{pmatrix} u_0 \\ v_0 \end{pmatrix} \mapsto \begin{pmatrix} u_0 + (1+r)(\Delta v_0) \\ v_0 - (1+r)v_0\sqrt{1 - \frac{2A_0u_0}{v_0^2}} \end{pmatrix} \tag{3.9}$$

where $\Delta > 0$ is the (small) time taken for the particle to travel from the Poincaré surface at $t = 0$ to the impact wall at $u = 0$. The above discontinuity map can be easily derived by keeping terms which are neglected when the map (3.8) is derived, see [10] for details. Note that the map for v_0 in equation (3.9) is exactly the same as in equation (3.8) as $\sqrt{v_0^2} = -v_0 \geq 0$. The expression $v_0^2 - 2A_0u_0$ is important in determining the behaviour of an orbit and if $v_0^2 - 2A_0u_0 = 0$ then an orbit grazes. For $v_0^2 - 2A_0u_0 > 0$ an impact will occur and the magnitude of this quantity determines the velocity of the particle at impact. If $v_0^2 - 2A_0u_0$ is small and positive then the square-root term in equation (3.8) becomes dominant and equation (3.8) is a good approximation to the discontinuity map. However, if $v_0^2 - 2A_0u_0$ is large and positive then Δ is approximately given by $\Delta = -u_0/v_0$ and if $\frac{2A_0u_0}{v_0^2} \ll 1$ then we simplify

equation (3.9) to the following linear map

$$P_{ZDM} : \begin{pmatrix} u_0 \\ v_0 \end{pmatrix} \mapsto \begin{pmatrix} -ru_0 \\ -rv_0 \end{pmatrix}. \tag{3.10}$$

We note that a similar linear discontinuity map for the impact oscillator is described in [13] and is derived in [10] by assuming that the path of the particle near the impact wall is linear. Thus the stroboscopic map for the case when $v_0^2 - 2A_0u_0$ is large and positive, which relates to an orbit impacting at high-velocity, is given as

$$\boldsymbol{w}_1 = P_T \circ P_{ZDM}(\boldsymbol{w}_0) = -rD\boldsymbol{w}_0 + \boldsymbol{g}. \tag{3.11}$$

3.2.4. One-dimensional approximation and regularisation. Above we have a stroboscopic map if either $v_0^2 - 2A_0u_0 < 0$ (non-impacting case) or if $v_0^2 - 2A_0u_0$ is large and positive (high-velocity impacting case). We do not yet have a map for the case when $v_0^2 - 2A_0u_0$ is small and positive which is normally the region in which the nonlinear discontinuity map (3.8) is applied but our approach is to regularise this region using the assumption that the stroboscopic map is continuous everywhere and that the map takes a square-root form for small positive values of $v_0^2 - 2A_0u_0$. First we reduce the maps (3.6) and (3.11) to a one-dimensional approximation and we do this using the same technique which is described in [17] and [18] and introduce the coordinate transformation $(u, v) \to (x, y)$ which is given as

$$x = v^2 - 2Au, \qquad y = -[dx + 2Abv + 2A(dg_1 - bg_2)] \tag{3.12}$$

where constants a, b, c, d, g_1 and g_2 are given by equation (3.7).

If an orbit has position u_0, velocity v_0 and acceleration A_0 at time $t = 0$ and $x_0 = v_0^2 - 2A_0u_0 < 0$ then the orbit will not impact during the time period $[0, T]$ and the stroboscopic map in terms of x and y using the coordinate transformation (3.12) and map (3.6), after some manipulation, is given as

$$x_1 = (a + d)x_0 + y_0 + 2A_0[(dg_1 - bg_2) - g_1], \qquad y_1 = -(ad - bc)x_0. \tag{3.13}$$

Now $ad - bc = \det(e^{BT}) = e^{\text{trace}(BT)} = e^{-\alpha T}$ and thus if αT is large then y_i terms can be neglected and a one-dimensional map in terms of x only is obtained. For $v_0^2 - 2A_0u_0$ large and positive (high-velocity impacting orbits) the map in the new coordinate system is

$$x_1 = -r(a + d)x_0 - ry_0 - 2A_0[r(dg_1 - bg_2) + g_1], \qquad y_1 = r(ad - bc)x_0 \tag{3.14}$$

and similarly, if αT is large then y_i terms are negligible. Therefore, if we now consider the general map from $t = nT$ to $t = (n + 1)T$, we have the system of one-dimensional maps,

$$x_{n+1} = \begin{cases} (a + d)x_n + 2A_n[(dg_1 - bg_2) - g_1] & \text{if } x_n < 0 \\ -r(a + d)x_n - 2A_n[r(dg_1 - bg_2) + g_1] & \text{if } 0 \ll \bar{x} < x_n. \end{cases}$$

Here the constant value $\bar{x}$ is introduced to separate between impacting orbits which impact with high- and low-velocity. We now wish to regularise this one-dimensional map such that it is continuous everywhere and takes a square root form in the region $0 < x_n < \bar{x}$. Before we do this, we first introduce the following parameters

$$\mu = 2A[(dg_1 - bg_2) - g_1] \qquad l = 2A(1 + r)(dg_1 - bg_2) \qquad \lambda_1 = a + d \tag{3.15}$$

which allows us to re-write the above map in the standard form

$$x_{n+1} = \begin{cases} \lambda_1 x_n + \mu & \text{if } x_n < 0 \\ -r\lambda_1 x_n + \mu - l & \text{if } \bar{x} < x_n. \end{cases} \tag{3.16}$$

Imposing the condition that the map is continuous at $x_n = \{0, \bar{x}\}$ and that the first derivative of the map is continuous at $x_n = \bar{x}$ leads us to the following regularised map in the region $0 < x < \bar{x}$,

$$x_{n+1} = -l\sqrt{\frac{4x_n}{\bar{x}}} + \left(\frac{l}{\bar{x}} - r\lambda_1\right) x_n + \mu \text{ if } 0 < x_n < \bar{x}.$$

Rescaling x_n by letting $\hat{x}_n = x_n/l$, $\epsilon = \bar{x}/l$ and $\hat{\mu} = \mu/l$, gives us the following map (immediately dropping the $\hat{}$s) which has a unit discontinuity

$$x_{n+1} \equiv f(x_n; \lambda_1, \mu, \epsilon) = \begin{cases} f_1(x_n) = \lambda_1 x_n + \mu, & \text{if } x_n < 0, \\ f_2(x_n) = -\sqrt{\frac{4x_n}{\epsilon}} + \left(\lambda_2 + \frac{1}{\epsilon}\right) x_n + \mu, & \text{if } 0 \le x_n < \epsilon, \\ f_3(x_n) = \lambda_2 x_n + \mu - 1, & \text{if } \epsilon \le x_n. \end{cases} \tag{3.17}$$

For the impact oscillator, see Figure (2.5), we have $\lambda_2 = -r\lambda_1$ and when we study the dynamics in more detail in §5 we consider the more general case $\lambda_2 < 0 < \lambda_1$. A plot of the map (3.17) is given in Figure (3.6).

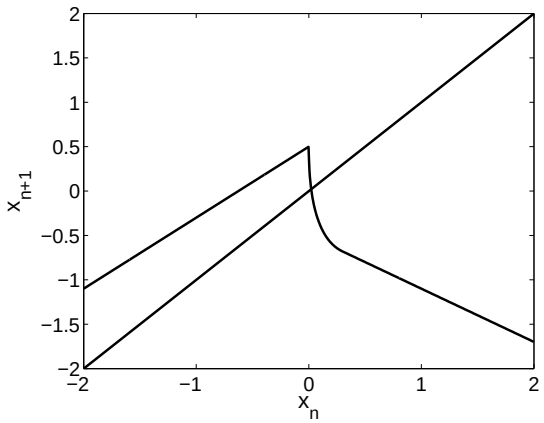

Fig. 3.6: A plot of the map (3.17) for $\lambda_1 = 0.8, \lambda_2 = -0.6, \epsilon = 0.3$ and $\mu = 0.5$. This map has a similar form to that of the stroboscopic map of the impact oscillator plotted in Figure (2.5) and denoted by the solid line.

4. Period-adding: $0 < \lambda < 1$ **(Cam-follower).** We now study the dynamics of the regularised discontinuous map (3.3) which was derived from the Poincaré map associated with those impacts of the cam-follower system occuring close to a corner. We first show that the map (3.3) produces similar bifurcation diagrams to the cam-follower system and then investigate the bifurcations which occur for the map (3.3). We note that in this case $\lambda_1 = \lambda_2 \equiv \lambda > 0$ which infers that the map is of period-adding type for the cam-follower. We recall that the value of ϵ decreases as the

curvature of the corner increases and that the case $\epsilon = 0$ corresponds to the example studied in [7] which is when the cam profile has a discontinuous first derivative. The key results of this section are a series of calculations showing the change in the existence regions for periodic orbits as ϵ changes from $\epsilon = 0$ to $\epsilon > 0$. This allows us to estimate for a given value of ϵ the largest value of N for which a period-N orbit can be observed.

A plot of the ω-limit sets (bifurcation diagram) for $\epsilon = 0$ and $\epsilon = 0.05$ is given in Figure (4.1) for $\lambda = 0.8 > 0$. The case $\epsilon = 0$ leads directly to a piecewise-linear

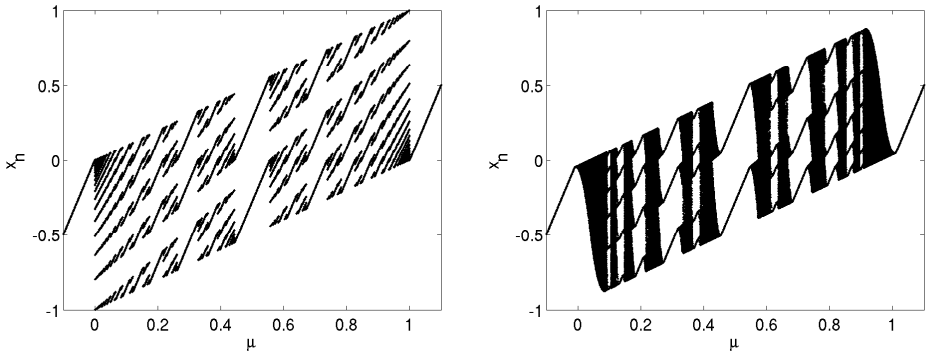

(a) $\epsilon = 0$ (b) $\epsilon = 0.05$

Fig. 4.1: The bifurcation diagrams for the regularised discontinuous map (3.3) with bifurcation parameter μ for $\lambda = 0.8$.

discontinuous map and has been extensively studied in the research literature and for more details see [2] [3] [4] [14] [15] but we briefly summarise the main results here. The principle orbits are periodic cycles $\{x_1, x_2, \ldots x_N\}$ which can be described via their symbolic sequences. In particular, if an iterate x_i of a periodic orbit occurs to the *left* of the discontinuity so that $x_i < 0$ we denote this by $\mathcal{L}$ and if it lies to the *right* it is denoted by $\mathcal{R}$. As an example, a period-7 orbit with six iterates to the left followed by one to the right has the symbolic expression $\mathcal{L}^6\mathcal{R}$. Discontinous (border-collision) bifurcations occur when one of the iterates x_i crosses the discontinuity boundary as a parameter varies so that a discontinuous bifurcation occurs when $x_i = 0$. In a period-adding bifurcation diagram, as shown in Figure (4.1a), we typically see period n orbits of symbolic sequence $\mathcal{L}^{n-1}\mathcal{R}$ followed by period m orbits of symbolic sequence $\mathcal{L}^{m-1}\mathcal{R}$ with a concatenated period $n+m$ orbit of symbolic sequence $\mathcal{L}^{n-1}\mathcal{R}\mathcal{L}^{m-1}\mathcal{R}$ lying inbetween. The winding number of such orbits (expressing the fraction of the time to the left of the discontinuity as a fraction of the overall period) then follows a *Farey Sequence* and more details on this can be found in [3] [10] [16]. The simplest period-N orbit to analyse are the (so called) *maximal orbits* of the form $\mathcal{L}^{N-1}\mathcal{R}$ for which $x_1, x_2, \ldots x_{N-1} < 0$ and $x_N > 0$. Repeated applications of the map (3.3) imply that

$$x_N = \lambda^{N-1}x_1 + \left(\frac{\lambda^{N-1} - 1}{\lambda - 1}\right)\mu, \quad x_1 = \lambda x_N + \mu - 1. \tag{4.1}$$

As $x_1 < x_2 < \ldots x_{N-1} < 0 < x_N$ it follows that such an orbit exists provided that μ

lies in the interval

$$\mu_{N,1} \equiv \frac{\lambda^{N-1}(1-\lambda)}{1-\lambda^N} < \mu < \frac{\lambda^{N-2}(1-\lambda)}{1-\lambda^N} \equiv \mu_{N,2}. \tag{4.2}$$

Border-collision bifurcations occur when $\mu = \mu_{N,1}$ and $x_N = 0$ or when $\mu = \mu_{N,2}$ and $x_{N-1} = 0$. The resulting intervals of existence for these maximal orbits and the complex transitions and period-adding sequences between them are visible in Figure (4.1a). We now consider the corresponding bifurcation diagram for the regularised map shown in Figure (4.1b). The main difference between the bifurcation diagrams arising when $\epsilon = 0$ and when $\epsilon = 0.05$ (for the same values of λ) is that chaotic intervals separate periodic intervals for $\epsilon = 0.05$ but only periodic orbits exist for $\epsilon = 0$. Furthermore, the orbits of higher period do not appear to persist as ϵ increases. We observe that the bifurcation figure for the cam-follower system, Figure (2.4), displays exactly the same qualitative structure as is shown in Figure (4.1b) and Figure (4.2). That is, between each periodic interval there exists a region of chaos and the sequence of periodic orbits in Figure (2.4) agrees with the period-adding sequence. In Figure (4.2) we plot two bifurcation diagrams for different values of ϵ and for $\mu \approx 0.07$ each plot contains a period-7 orbit which is a smooth continuation of one of symbol sequence $\mathcal{L}^6\mathcal{R}$ arising when $\epsilon = 0$. Observe that for $\epsilon = 0.01$ we see orbits of periods 6 to 12 whilst for $\epsilon = 0.04$ we see only those of periods 6 and 7 persist.

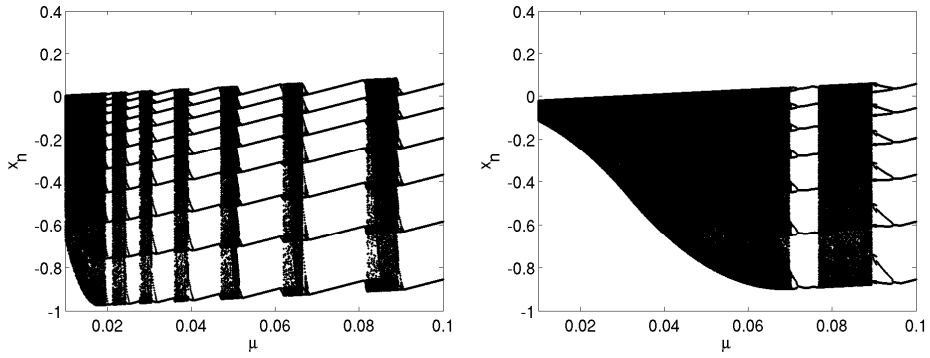

(a) $\epsilon = 0.01$, orbits of period 12 to 6 exist (b) $\epsilon = 0.04$, orbits of period 7 and 6 only exist

Fig. 4.2: Close-up bifurcation figures for $\lambda = 0.8$ for the map (3.3).

To understand the structure of the bifurcation diagrams for $\epsilon > 0$ we now investigate in more detail the nature of the bifurcations observable in Figure (4.2). When $\epsilon > 0$ the regularised map has continuous first derivatives and we expect the bifurcations of the periodic orbits to be (smooth) period-doubling or fold-bifurcations. In Figure (4.2a) we see that the existence regions for the periodic orbits are apparently bounded by period-doubling bifurcation points for values of μ rather larger than ϵ. However, in the limit $\epsilon = 0$ all bifurcations are (nonsmooth) border-collision type bifurcations which arise as we have seen when an iterate of the orbit intersects the discontinuity. To analyse this we again consider the maximal periodic orbits of the symbolic sequence $\mathcal{L}^{N-1}\mathcal{R}$ when $\epsilon = 0$ and determine for which values of μ smooth perturbations of orbits exist as ϵ increases. (We note that a simple symmetry argument also determines when orbits of the form $\mathcal{L}\mathcal{R}^{N-1}$ exist.) For example, consider the orbits in Figure (4.2b)

arising when $\epsilon = 0.04$, the period 6 orbit which exists for $\mu = 0.1$ appears to have a period-doubling bifurcation at $\mu \approx 0.095$ and persists locally for $\mu > 0.095$ before vanishing, in this case at a fold bifurcation. Instead of the border-collision bifurcation at $\mu = \mu_{N,1}$, we consistently appear to have a period-doubling bifurcation for a slightly perturbed value of $\mu = \mu_{PD,N,1}$. This arises when the (corresponding) point x_N of the orbit lies in the (regularisation) interval in which the map, though regular, has a high negative gradient. For the map described in (3.3) this implies that

$$x_N = f_1(x_{N-1}), \quad x_1 = f_3(x_N)$$

so that

$$x_N = \lambda^{N-1} x_1 + \left(\frac{\lambda^{N-1} - 1}{\lambda - 1} \right) \mu, \quad x_1 = \frac{x_N^2}{2\epsilon^2} + (\lambda - 1/\epsilon) x_N + \mu - \frac{1}{2}. \tag{4.3}$$

If such a maximal orbit $\mathcal{L}^{N-1}\mathcal{R}$ exists for a certain value of μ then as μ is decreased there is a certain value of $\mu \equiv \mu_{PD,N}$ at which the orbit of type $\mathcal{L}^{N-1}\mathcal{R}$ undergoes a bifurcation. As $f_1' > 0$ and $f_3' < 0$ this must be a period-doubling bifurcation so that

$$(f_1')^{N-1} f_3'(x_N) = -1.$$

The form of such an orbit is shown in Figure (4.3). Using the explicit form of map

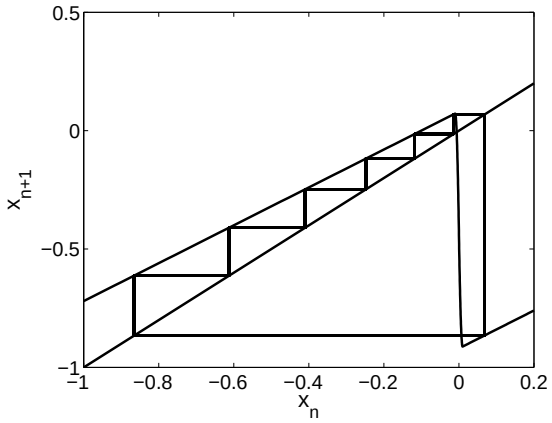

Fig. 4.3: A plot of the period-7 orbit close to undergoing a period-doubling bifurcation for parameters $\lambda = 0.8, \epsilon = 0.01$ and $\mu = 0.08$.

(3.3) it follows that

$$(f_1')^{N-1} f_3'(x_N) = \lambda^{N-1} \left(\frac{x_N}{\epsilon^2} + \lambda - \frac{1}{\epsilon} \right) = -1.$$

If we consider the case of $\epsilon \ll \lambda$ then, after some manipulation,

$$x_N = \epsilon - \epsilon^2 \left(\lambda + \lambda^{1-N} \right), \quad x_1 = \mu - 1 + \lambda\epsilon + \mathcal{O}(\epsilon^2).$$

Hence, solving (4.3) for μ we have

$$\mu_{PD,N,1} = \frac{\lambda^{N-1}(1-\lambda)}{1-\lambda^N} + (1-\lambda)\epsilon + \mathcal{O}(\epsilon^2).$$

Observe that $\mu_{PD,N,1} = \mu_{N,1} + \mathcal{O}(\epsilon) > \mu_{N,1}$.

If we now increase μ from $\mu_{PD,N,1}$ the periodic orbit will again cease to exist at a bifurcation. This can arise in one of two ways: through a period-doubling bifurcation at a fixed point of the iterated map $f_1^{N-2} \circ f_2 \circ f_4$ (which is a perturbation of the border-collision bifurcation arising when $x_{N-1} = 0$), or alternatively, at a saddle-node bifurcation at a fixed point of the iterated map $f_1^{N-2} \circ f_2 \circ f_3$. The latter case arising when $\mu = \mathcal{O}(\epsilon)$.

The analysis of the first case, in which μ is rather greater than ϵ, proceeds much as above and we have $x_1 = f_4(x_N), x_N = f_2(x_{N-1}), x_{N-1} = f_1(x_{N-2})$. Setting $(f_1^{N-2})' f_2' f_4' = -1$ gives $x_{N-1} = -\epsilon + \epsilon^2(\lambda + \lambda^{1-N})$ and $x_N = \mu - \lambda\epsilon + \mathcal{O}(\epsilon^2)$. So that if ϵ is small then x_{N-1} lies inside the 'regularisation' interval and x_N lies outside it provided $x_N > \epsilon$. This condition is satisfied when

$$\mu > (1 + \lambda)\epsilon + \mathcal{O}(\epsilon^2).$$

Hence, repeating the above analysis in this case, there is a period-doubling bifurcation when

$$\mu \equiv \mu_{PD,N,2} = \frac{\lambda^{N-2}(1-\lambda)}{1-\lambda^N} - (1-\lambda)\epsilon + \mathcal{O}(\epsilon^2). \tag{4.4}$$

Again observe that $\mu_{PD,N,2} = \mu_{N,2} - \mathcal{O}(\epsilon) < \mu_{N,2}$.

We now examine the case of $\mu < (1 + \lambda)\epsilon$ in which both of the iterates x_{N-1} and x_N lie inside the 'regularisation' interval so that $x_N = f_2(x_{N-1}), x_1 = f_3(x_N)$. This case is illustrated in Figure (4.4). The iterated map is now $(f_1^{N-2}) \circ f_2 \circ f_3$ and as

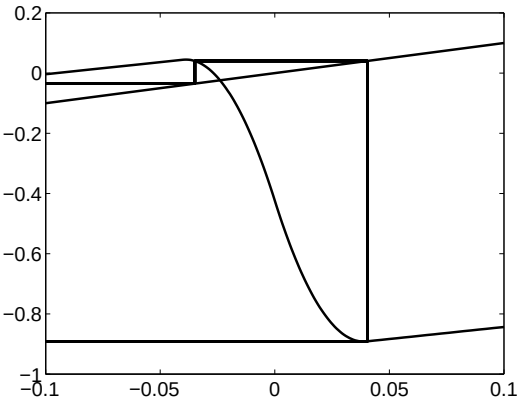

Fig. 4.4: An orbit close to undergoing a fold-bifurcation for the map (3.3) for parameters $\lambda = 0.8, \mu = 0.0765$ and $\epsilon = 0.04$.

$f_1' > 0, f_2' < 0, f_3' < 0$ this orbit ceases to exist at a saddle-node bifurcation for which $(f_1^{N-2})' f_2' f_3'(x_N) = 1$ which explicitly is

$$\lambda^{N-2}\left(-\frac{x_{N-1}}{\epsilon^2} + \lambda - \frac{1}{\epsilon}\right)\left(\frac{x_N}{\epsilon^2} + \lambda - \frac{1}{\epsilon}\right) = 1.$$

As μ increases then x_{N-1} increases and when $x_{N-1} \approx -\epsilon$ a saddle-node bifurcation occurs. For x_N to lie in the regularisation interval with $x_N > 0$ we must have $x_N = a\epsilon$ for some $0 < a < 1$. Substituting into the above expression this implies that a saddle-node bifurcation occurs when

$$x_{N-1} = -\epsilon + \lambda\epsilon^2 - \frac{\epsilon^3\lambda^{2-N}}{(a-1)} + \mathcal{O}(\epsilon^4).$$

Furthermore, as $x_N = f_2(x_{N-1})$, then

$$\mu = (1+a)\epsilon + \mathcal{O}(\epsilon^2).$$

It further follows that

$$x_1 = f_3(x_N) = \mu + (a^2-1)/2 - a + \lambda a\epsilon \quad \text{and} \quad x_{N-1} = -\epsilon + \mathcal{O}(\epsilon^2) = \lambda^{N-2}x_1 + \frac{(1-\lambda^{N-2})\mu}{1-\lambda}.$$

We have, after combining these expressions and some manipulation, that at the saddle-node bifurcation $\mu \equiv \mu_{SN,N}$ and satisfies the equation

$$\mu_{SN,N} = \frac{\lambda^{N-2}(1-\lambda)}{1-\lambda^{N-1}}(a + (1-a^2)/2) - \frac{\epsilon(1+a\lambda^{N-1})(1-\lambda)}{1-\lambda^{N-1}} + \mathcal{O}(\epsilon^2),$$

and as $0 < a < 1$ we have

$$\mu_{SN,N} < \frac{\lambda^{N-2}(1-\lambda)}{1-\lambda^{N-1}} - \frac{\epsilon(1-\lambda)}{1-\lambda^{N-1}} + \mathcal{O}(\epsilon^2).$$

We have seen in Figures (4.1) and (4.2) that as ϵ increases the total number of periodic orbits which exist decreases. This occurs because the width of the intervals $(\mu_{PD,N,1}, \mu_{SN,N})$ and $(\mu_{PD,N,1}, \mu_{PD,N,2})$ decrease as ϵ increases and eventually become zero at which point the orbit vanishes. From the expressions for $\mu_{PD,N,1}$ and $\mu_{SN,N}$ we can approximate the value of ϵ for which an orbit of the form $\mathcal{L}^{N-1}\mathcal{R}$ vanishes by

$$\epsilon_N = \frac{\lambda^{N-2}(1-\lambda)}{(1-\lambda^N)(2-\lambda^{N-1})}. \tag{4.5}$$

Note that, as observed, ϵ_N decreases as N increases. A numerical plot of the transition of the periodic orbit $\mathcal{L}^6\mathcal{R}$ as ϵ increases is plotted in Figure (4.5). Observe that the period-7 orbit is stable for small values of ϵ and vanishes at a saddle-node bifurcation as ϵ increases. A numerical calculation indicates that this occurs when $\epsilon = 0.043$. Our prediction is $\epsilon_7 = 0.048$ which shows good agreement.

Similarly, it follows from equation (4.5) that if ϵ is fixed then the largest value of N for which we expect to see a period-N orbit is given approximately by

$$N_{max} = 2 + \frac{\log(2\epsilon/(1-\lambda))}{\log(\lambda)}.$$

For example, if $\lambda = 0.8$ and $\epsilon = 0.03$ then $N_{max} \approx 7.39$. In Figure (4.6) we give a bifurcation diagram for these values and can clearly see that the largest observed orbit has period-8, in good agreement with the result above.

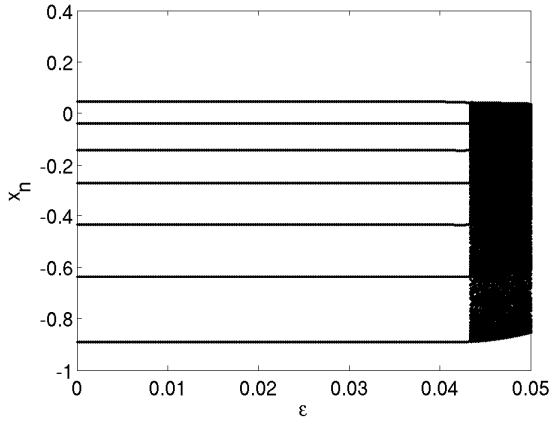

Fig. 4.5: The bifurcation diagram for the map (3.3) when ϵ is the parameter. The parameters are $\lambda = 0.8$ and $\mu = 0.075$ and as ϵ increases the period-7 orbit vanishes when $\epsilon = 0.043$.

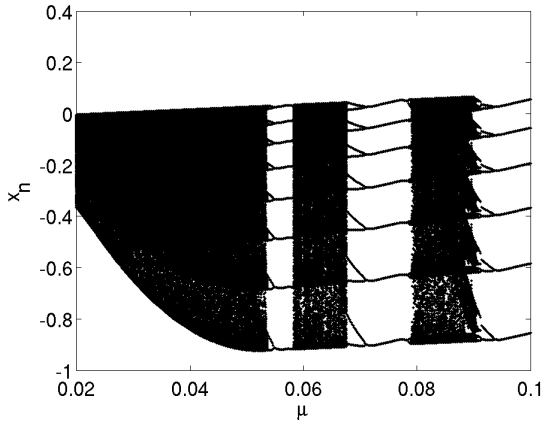

Fig. 4.6: A bifurcation diagram showing the existence of a period-8 orbit but not a period-9 orbit which agrees with our analysis, the parameters are $\lambda = 0.8$ and $\epsilon = 0.03$.

We have seen in this section how a regularised one-dimensional discontinuous map can approximate the behaviour of a cam-follower system with impacts occuring close to a smooth but sharp corner of the cam. The bifurcation diagrams of the regularised one-dimensional map are qualitatively similar to the bifurcation diagrams for the cam-follower system. To increase accuracy a regularised two-dimensional discontinuous map would improve quantative agreement between the model and the approximation. However, this would be challenging as the dynamics of a discontinuous two-dimensional map are as yet not understood.

5. Period-incrementation: $\lambda_1\lambda_2 \equiv -r\lambda^2 < 0$ (Impact Oscillator). We now study the dynamics of the regularised discontinuous map (3.17) which was derived by

considering the linear dynamics of high-velocity impacting orbits and regularising the map to capture the local nonlinear effects of low-velocity impacts. A feature of the map (3.17) which gives it different behaviour to the map (3.3) derived for the cam-follower system is that the slopes of the respective linear parts are positive-negative for the impact oscillator but are positive-positive for the cam-follower system. Hence we expect to see period-incrementing behaviour in this case.

In Figure (2.6) we plotted a bifurcation diagram calculated directly from the impact oscillator system and in Figure (5.1) we have used equivalent parameter values, calculated using equation (3.15). Figures (2.6) and (5.1) are very similar (qualitatively) and we can see that the ratio of the widths of the regions of existence for the period-2 and period-3 orbits are similar, with clear evidence of period-incrementing behaviour.

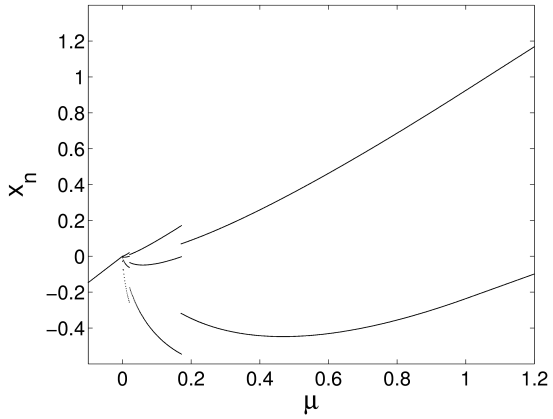

Fig. 5.1: The bifurcation diagram for the ω-limit sets for map (3.17) with parameter values $\lambda_1 = 0.32, \lambda_2 = -0.26$ and $\epsilon = 0.93$.

As in the previous section we now consider the effect of the regularisation on the map with a gap, and in particular will see that certain high period orbits vanish as ϵ increases although the overall period-incrementing structure is maintained. For this analysis it is convenient to study a general system of the form (3.17) with $-1 < \lambda_2 < 0 < \lambda_1 < 1$.

The bifurcation diagrams of the ω-limit sets for the regularised discontinuous map (3.17) with fixed parameters $\lambda_1 = 0.7$ and $\lambda_2 = -0.9$ and $\epsilon = \{0, 0.1, 0.3, 1\}$ are plotted in Figure (5.2). In all of these figures we see period incrementing behaviour, but we note that (as before) the high period orbits which exist for small values of ϵ vanish and are replaced by chaotic behaviour. Similarly, the overlapping intervals of existence of the period orbits are generally replaced by chaotic intervals.

The limiting case of the map with a gap when $\epsilon = 0$ has been studied in [14] and details of this case can be found in [10] and [14]. To briefly summarise these results (for which the analysis is very similar to that of the previous section), we can study the maximal periodic orbits of the form $\mathcal{L}^{N-1}\mathcal{R}$ with $x_1, \ldots x_{N-1} \in \mathcal{L}$ and $x_N \in \mathcal{R}$

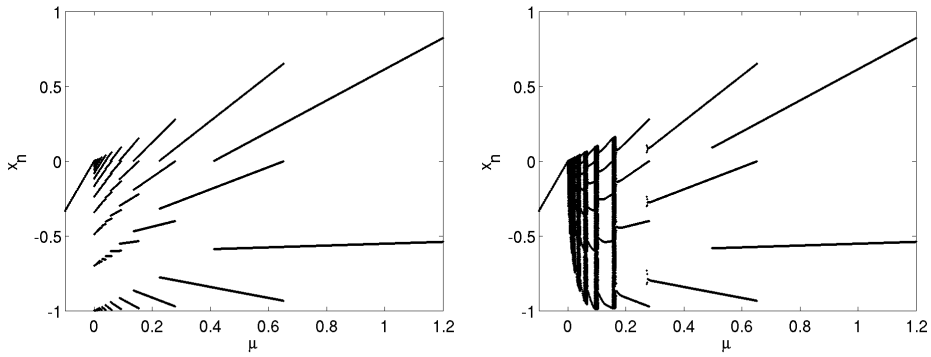

(a) $\epsilon = 0$ (b) $\epsilon = 0.1$

(c) $\epsilon = 0.3$ (d) $\epsilon = 1$

Fig. 5.2: The bifurcation diagram for the ω-limit sets of map (3.17) with parameters $\lambda_1 = 0.7$ and $\lambda_2 = -0.9$.

so that

$$x_N = \lambda_1^{N-1} x_1 + (1 - \lambda_1^{N-1})\mu/(1 - \lambda_1), \quad x_1 = \lambda_2 x_N + \mu - 1.$$

Such orbits arise at border-collision bifurcation points $\mu_{N,1}$ ($x_N = 0$) and $\mu_{N,2}$, ($x_{N-1} = 0$) given by

$$\mu_{N,1} = \frac{\lambda_1^{N-1}(1 - \lambda_1)}{1 - \lambda_1^N}, \quad \mu_{N,2} = \frac{\lambda_1^{N-2}(1 - \lambda_1)}{1 - \lambda_1^{N-2}(\lambda_1\lambda_2 + (\lambda_1 - \lambda_2))}.$$

When $\epsilon > 0$ these bifurcation points change in their nature with $\mu_{N,1}$ becoming a period-doubling bifurcation. Figure (5.2) clearly shows that as ϵ increases from 0 the number of different periodic orbits decreases and periodic orbits are replaced by chaotic intervals. Note that all periodic orbits in Figure (5.2) are of the form $\mathcal{L}^{N-1}\mathcal{R}$. Increasing ϵ has the effect of narrowing the width of the existence intervals of the periodic orbits and for large enough ϵ the periodic orbits vanish and are replaced by chaos.

We now derive the existence intervals for periodic orbits $\mathcal{L}^{N-1}\mathcal{R}$ in this case. An example of a period-6 orbit ($\mathcal{L}^5\mathcal{R}$) is plotted in Figure (5.3) and this orbit (and orbits

$\mathcal{L}^{N-1}\mathcal{R}$ in general) undergo a bifurcation if μ is increased and the largest negative iterate x_{N-1} collides with the discontinuity border and undergoes a border-collision bifurcation. Similarly, if μ is decreased then the point x_N moves into the regularisation interval (as seen in Figure (5.3)) and we have $x_1 = f_2(x_N), \quad x_N = f_1(x_{N-1})$. A period-doubling bifurcation then arises when

$$(f_1^{N-1})' f_2'(x_N) = -1.$$

Examples of this behaviour is given in Figure (5.5).

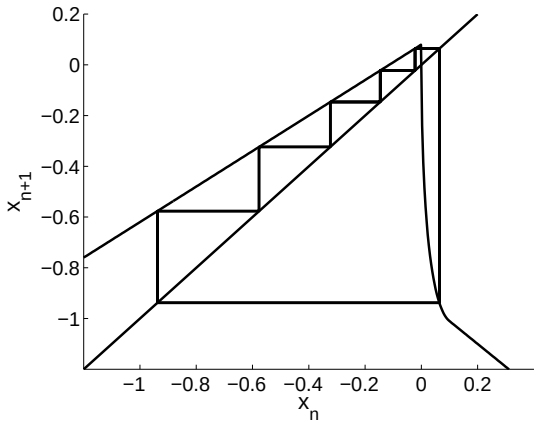

Fig. 5.3: A period-6 orbit for the map (3.17) for parameters $\lambda_1 = 0.7, \lambda_2 = -0.9, \epsilon = 0.1$ and $\mu = 0.08$.

A general $\mathcal{L}^{N-1}\mathcal{R}$ orbit undergoes a border-collision bifurcation at $\mu = \mu_{BC,N}$ when $x_{N-1}(\mu) = 0, x_N = \mu$. If $\mu > \epsilon$ then x_N lies outside of the regularisation interval and $x_1 = f_3(x_N)$ and exactly the same analysis as before (for $\epsilon = 0$) can be applied so that in this case the border collision occurs when $\mu_{BC,N} = \mu_{N,2}$. In the case of $\mu < \epsilon$ we have $x_1 = f_2(x_N)$ and following some algebra, the resulting value for $\mu_{BC,N}$ for the case $\mu < \epsilon$ is given by

$$\mu_{BC,N} = \frac{4\lambda_1^{2(N-2)}\epsilon}{\left\{(\lambda_2\epsilon + 1)\lambda_1^{N-2} + \epsilon\left(\frac{\lambda_1^{N-1}-1}{\lambda_1 - 1}\right)\right\}^2}.$$

The period-doubling bifurcation occurs when $\mu = \mu_{PD,N}$ at which $(f_1^{(N-1)})' f_2(x_N)' = -1$. Using the explicit form of map (3.17) the condition $(f_1^{(N-1)})' f_2(x_N)' = -1$ is

$$\lambda_1^{N-1}\left(\frac{-1}{\sqrt{\epsilon x_N}} + \lambda_2 + \frac{1}{\epsilon}\right) = -1$$

which can be rearranged to show that $x_N \approx \epsilon$. The iterate x_N satisfies the condition $f_1^{(N-1)} f_2(x_N) = x_N$ which is explicity

$$\lambda_1^{N-1}\left[-\sqrt{\frac{4x_N}{\epsilon}} + \left(\lambda_2 + \frac{1}{\epsilon}\right)x_N + \mu\right] + \left(\frac{\lambda_1^{N-1}-1}{\lambda_1 - 1}\right)\mu = x_N.$$

Calculated upto $\mathcal{O}(\epsilon)$ we have

$$\mu_{PD,N}(\epsilon) = \frac{\lambda_1^{N-1} - \lambda_1^N}{1-\lambda_1^N} + \frac{(1-\lambda_1)(1-\lambda_1^{N-1}\lambda_2)}{1-\lambda_1^N}\epsilon + \mathcal{O}(\epsilon^2).$$

Observe that $\mu_{PD,N} = \mu_{N,1} + \mathcal{O}(\epsilon) > \mu_{N,1}$.

If $\epsilon = 0$ we denote the existence intervals of the $\mathcal{L}^{N-1}\mathcal{R}$ orbit by I_N, for which $\mu \in (\mu_{N,1}, \mu_{N,2})$. These intervals are of non-zero width, and the intersection between I_N and I_{N+1} is non-empty. For $\epsilon > 0$ the width of the corresponding existence interval $I_N(\epsilon)$, for which $\mu \in (\mu_{PD,N}, \mu_{BC,N})$, is now a function of ϵ. As ϵ increases the width of the existence interval decreases and the orbit $\mathcal{L}^{N-1}\mathcal{R}$ does not exist for $\mu_{PD,N}(\epsilon) > \mu_{BC,N}(\epsilon)$. Similarly, the interval $I_N(\epsilon) \cap I_{N+1}(\epsilon)$ vanishes at some point as ϵ increases. This is illustrated in Figure (5.4) in which we plot the intervals in the cases of $N = 3, 4, 5$ by showing the paths of the period-doubling bufurcations (solid) and border-collision bifurcations (dashed) as ϵ increases. In this figure it can be seen that the period-3 orbit exists for $\epsilon < 0.65$ (approximately) and that the period-3 orbit coexists with the period-4 orbit for $\epsilon < 0.08$ (approximately). To illustrate this

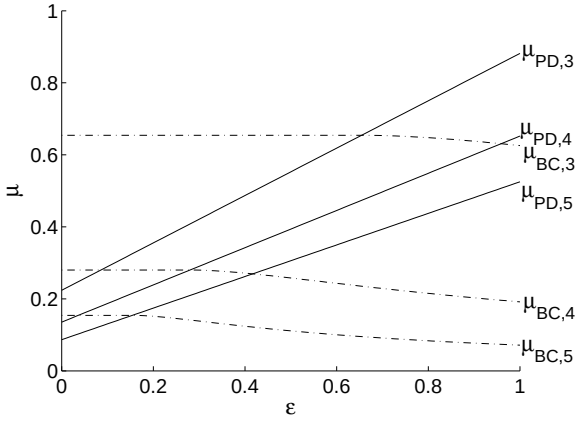

Fig. 5.4: A plot showing the values of μ for which period-doubling (solid lines) and border-collision bifurcations (dashed lines) occur for orbits with period $N = 3, 4, 5$. The parameters are $\lambda_1 = 0.7$ and $\lambda_2 = -0.9$.

further we plot in Figure (5.5) the bifurcation diagram when $\epsilon = 0.07$ in which we can see the co-existence of the period-3 and period-4 orbits for this value, but that the period-4 and period-5 orbits (and similarly the period-5 and period-6 orbits) are now separated by an interval of chaotic behaviour.

We have seen in this section how a regularised discontinuous piecewise-linear map which was derived using an outer approximation of the linear dynamics of the impact oscillator gives qualitatively good agreement with the actual model. We have also analysed the difference in behaviour between the discontinuous piecewise-linear map (1.1) and the regularised discontinuous map (3.17).

6. Conclusions. In this paper we have seen that the dynamics of a cam-follower system which impacts a smoothed corner can be described by a regularised discontinuous map and that the smooth bifurcations of such regularised discontinuous maps

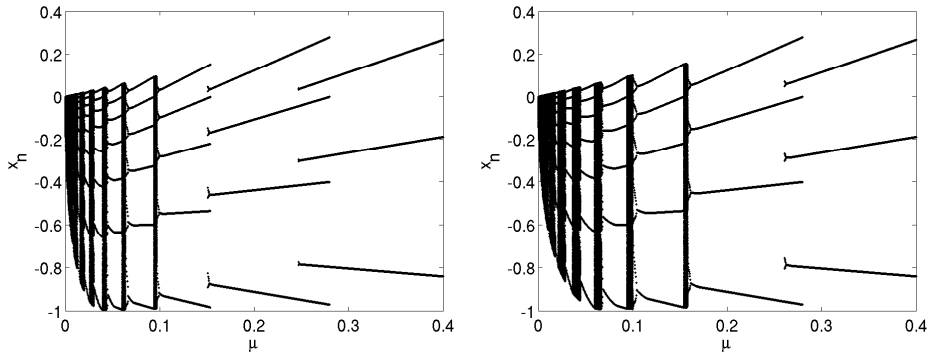

(a) $\epsilon = 0.04$ (b) $\epsilon = 0.07$

Fig. 5.5: Bifurcation diagrams for the map (3.17) for parameters $\lambda_1 = 0.7$ and $\lambda_2 = -0.9$ showing that for $\epsilon = 0.04$ the period-4 and period-5 orbit coexist but for $\epsilon = 0.07$ a region of chaos separates the two orbits. This agrees exactly with Figure (5.4) which plots the existence regions for the period-4 and period-5 orbits.

are 'close' to the nonsmooth border-collision bifurcations of a piecewise-linear discontinuous map. We have also shown that the stroboscopic map for the impact oscillator can be derived by considering the outer linear dynamics of the system and gives a regularised discontinuous map. The regularised discontinuous map produces bifurcation diagrams which are in reasonable agreement with bifurcation diagrams produced directly from the impact oscillator system. Our method of considering the outer linear dynamics could be tested on other discontinuity-type bifurcations where the local nonlinear effects are outweighed by the global linear behaviour of the system and the local nonlinear behaviour could be obtained by regularisation.

Acknowledgements. The authors would like to thank Professor M. di Bernardo for many helpful discussions regarding the cam-follower dynamics. SRP would like to acknowledge support from the Engineering and Physical Sciences Research Council. We would also like to thank the referees for their useful and insightful comments which have significantly improved the quality of this paper.

REFERENCES

[1] R. Alzate, M. di Bernardo, U. Montanaro, and S. Santini, *Experimental and numerical verification of bifurcations and chaos in cam-follower impacting systems*, Nonlinear Dynam., 50 (2007), pp. 409–429.

[2] V. Avrutin and M. Schanz, *On multi-parametric bifurcations in a scalar piecewise-linear map*, Nonlinearity, 19 (2006), pp. 531–552.

[3] V. Avrutin, M. Schanz, and S. Banerjee, *Multi-parametric bifurcations in a piecewise-linear discontinuous map*, Nonlinearity, 19 (2006), pp. 1875–1906.

[4] ———, *Codimension-three bifurcations: Explanation of the complex one-, two-, and three-dimensional bifurcation structures in nonsmooth maps*, Phys. Rev. E, 75 (2007), pp. 1875–1906.

[5] P. Bressloff and J. Stark, *Neuronal dynamics based on discontinuous circle maps*, Phys. Lett. A, 150 (1990), pp. 187–195.

[6] C. Budd and F. Dux, *Chattering and related behaviour in impact oscillators*, Philos. Trans. R. Soc. Lond. A, 347 (1994), pp. 365–389.

[7] C. Budd and P. Piiroinen, *Corner bifurcations in nonsmoothly forced impact oscillators*, Phys. D, 220 (2006), pp. 127–145.
[8] D. Chillingworth, *Discontinuity geometry for an impact oscillator*, Dyn. Syst., 17 (2002), pp. 389–420.
[9] W. Chin, E. Ott, C. Grebogi, and H. Nusse, *Grazing bifurcations in impact oscillators*, Phys. Rev. E, 50 (1994), pp. 4427–4444.
[10] M. di Bernardo, C. Budd, A. Champneys, and P. Kowalczyk, *Piecewise-smooth Dynamical Systems: Theory and Applications*, Springer, 2008.
[11] M. di Bernardo, M. Feigin, S. Hogan, and M. Homer, *Local analysis of c-bifurcations in n-dimensional piecewise-smooth dynamical systems*, Chaos, Solitons and Fractals, 10 (1999), pp. 1881–1908.
[12] S. Foale and S. Bishop, *Bifurcations in impact oscillators*, Nonlinear Dynam., 6 (1994), pp. 285–299.
[13] M. H. Fredriksson and A. B. Nordmark, *On normal form calculations in impact oscillators*, Proc. R. Soc. Lond. Ser. A Math. Phys. Eng. Sci., 456 (2000), pp. 315–329.
[14] S. Hogan, L. Higham, and T. Griffin, *Dynamics of a piecewise linear map with a gap*, Proc. R. Soc. Lond. Ser. A Math. Phys. Eng. Sci, 463 (2007), pp. 49–65.
[15] P. Jain and S. Banerjee, *Border-collision bifurcations in one-dimensional discontinuous maps*, Internat. J. Bifur. Chaos Appl. Sci. Engrg., 13 (2003), pp. 3341–3351.
[16] J. Keener, *Chaotic behaviour in piecewise continuous difference equations*, Trans. Amer. Math. Soc., 261 (1980), pp. 589–604.
[17] J. Molenaar, J. de Weger, and W. van de Water, *Mappings of grazing-impact oscillators*, Nonlinearity, 14 (2001), pp. 301–321.
[18] A. Nordmark, *Non-periodic motion caused by grazing incidence in impact oscillators*, J. Sound Vibration, 145 (1991), pp. 279–297.
[19] ———, *Universal limit mapping in grazing bifurcations*, Phys. Rev. E, 55 (1997), pp. 266–270.
[20] ———, *Existence of periodic orbits in grazing bifurcations of impacting mechanical oscillators*, Nonlinearity, 14 (2001), pp. 1517–1542.
[21] G. Osorio, M. di Bernardo, and S. Santini, *Corner-impact bifurcations: A novel class of discontinuity-induced bifurcations in cam-follower systems*, SIAM J. Appl. Dyn. Syst., 7 (2008), pp. 18–38.